




Investigation of Internal Cracks in Epoxy-Alumina Using In Situ Mechanical Testing Coupled with Micro-CT

YICHUN TANG,^{1,3} KANGNING SU,^{1,4} RUYI MAN,^{1,5}
MICHAEL C. HILLMAN,^{2,6} and JING DU^{1,7} 

1.—Department of Mechanical Engineering, Pennsylvania State University, University Park, PA 16802, USA. 2.—Department of Civil and Environmental Engineering, Pennsylvania State University, University Park, PA, USA. 3.—e-mail: yzt5124@psu.edu. 4.—e-mail: kxs535@psu.edu. 5.—e-mail: rxm5330@psu.edu. 6.—e-mail: mhillman@psu.edu. 7.—e-mail: jingdu@psu.edu

Polymer-ceramic composites are widely used in biomedical applications. This paper presents the results of an experimental investigation on the crack extension inside epoxy-alumina. Specimens with 5 vol.%, 10 vol.%, ..., 25 vol.% fillers fractions were fabricated. Three-point bending on single-edge notched bend specimens were performed using conventional mechanical tester and in situ mechanical tester coupled with micro-CT, respectively. Fracture toughness was measured to be 2.10–2.51 MPa√m, and it decreased with increasing filler fraction. When cracks were shorter than 0.88 mm, crack resistance for 5 and 25 vol.% epoxy-alumina was similar. Beyond 0.88 mm, 25 vol.% epoxy-alumina exhibited no crack resistance, whereas stress intensity factor kept increasing in 5 vol.% epoxy-alumina. The matrix-particle interfaces were the weakest link, where cracks often initiated from. Crack bridging by uncracked ligament and crack deflection were commonly observed toughening mechanisms. To design robust epoxy-alumina composites, increasing matrix-particle interface strength is recommended for future work.

INTRODUCTION

Polymer-ceramic composite materials are widely used in biomedical applications, such as tissue engineering scaffolds,¹ orthopedic implants,² and drug delivery devices.³ In our prior works, epoxy-zirconia and epoxy-alumina composites were used in the bio-inspired design of functionally graded materials for dental restoration crowns.^{4,5} The critical loads under contact loading in the structures fabricated using these composite materials were found to be about 20–40% greater than those in the conventional structures using commercially available dental adhesive materials. The load-bearing capacity of these structures are related to the fracture properties of composites, which have not been fully explored.

The recent developments of x-ray based imaging techniques have provided new opportunities to study internal damage and cracks in composite

materials. Synchrotron radiation computed tomography (SR-CT) has been used to investigate fracture in natural composite materials, such as dentin⁶ and bone.⁷ Micro x-ray computed tomography (micro-CT) was used to study the internal damage in polymer-fiber composites.⁸ In situ mechanical testing coupled with SR-CT revealed damage mechanisms in epoxy-fiber laminates.⁹ In situ mechanical testing coupled with micro-CT was used to measure the three-dimensional (3D) deformation in carbon fiber reinforced polymer composite¹⁰ and 3D internal strain in bone.^{11,12}

In this paper, the internal crack growth was studied in a model polymer-ceramic composite system, epoxy-alumina, using in situ mechanical testing coupled with micro-CT. The fracture toughness of pure epoxy and epoxy-alumina containing 5 vol.%, 10 vol.%, ... 25 vol.% alumina fillers were measured, respectively. The crack growth resistance curves (R-curves) were obtained for 5 vol.% and 25 vol.% epoxy-alumina composites. The crack paths and crack toughening mechanisms were

(Received February 7, 2021; accepted April 26, 2021)

revealed by the micro-CT images. The implications of the results are then discussed for the design of more robust epoxy-alumina composites and for the experimental methods of studying cracks in composites.

MATERIALS AND METHODS

Sample Preparation

The epoxy-alumina composite specimens were fabricated by mixing epoxy matrix (EPO-TEK 301, Epoxy Technology Inc., Brillerica, MA) with 180-grit ($\sim 82 \mu\text{m}$) alumina particles (Saint-Gobain, Worcester, MA). Mixtures containing 5 vol.%, 10 vol.%, 15 vol.%, 20 vol.% and 25 vol.% alumina, respectively, were prepared. The volume percentage was estimated using the weight of each component measured by a scale, the specific gravity of the epoxy, 1.09, provided by the manufacturer, and the density of alumina, 3.97 g/cm^3 .¹³

After mixing, the mixture was poured into a silicon rubber mold (Allied High Tech Products Inc., Rancho Dominguez, CA) and degassed in a vacuum chamber for 20 min. It was then removed from the vacuum and stirred for 2–5 min. The degassing and stirring cycles repeated for $\sim 3 \text{ h}$. Then the mixture was cured in an oven at 100°C for 30 min. The optical image for a thin slice of a representative epoxy-alumina specimen (Fig. 1a) shows that the specimens did not contain visible gas bubbles and the alumina particles were evenly distributed in the matrix. Pure epoxy specimens were also fabricated using similar method.

Single-edge notched bend (SENB) specimens were prepared according to ASTM standard E399.¹⁴ They were cut using a diamond saw (Isomet 1000 Precision Cutter, Buehler, Lake Bluff, IL) and then polished using a grinder polisher (MetaServ® 250, Buehler, Lake Bluff, IL) with 120-grit sandpaper. The SENB specimens were $\sim 5 \times 5 \times 25 \text{ mm}^3$. The length of initial notch was measured using an optical microscope (ProScope, Bodelin Technologies, Oregon City, OR) to be about half of the specimens' width.

Three-Point Bend Using Conventional Mechanical Tester

Three-point bending tests were performed on the epoxy-alumina specimens using a mechanical testing machine (Electro E3000, Instron, Norwood, MA) with a loading span of 20 mm (Fig. 1b). They were conducted in air at room temperature. Four to five specimens were tested for each volume fraction of the epoxy-alumina specimens and for pure epoxy specimens, respectively. They were loaded monotonically to failure under displacement control at a cross-head speed of 0.1 mm/min . The loads and displacements were recorded by the tester.

The stress intensity factor is given by¹⁴

$$K_I = \frac{PS}{BW^{3/2}} \times f\left(\frac{a}{W}\right) \quad (1)$$

where P is the applied load; S , a , B , W are the span, notch length, thickness, and width of the SENB specimens, respectively; $f(\frac{a}{W})$ is the compliance function, given by¹⁵

$$f\left(\frac{a}{W}\right) = 3\sqrt{\frac{a}{W}} \times \frac{1.99 - (\frac{a}{W}) \times (1 - \frac{a}{W}) \times [2.15 - 3.93\frac{a}{W} + 2.7(\frac{a}{W})^2]}{2(1 + 2\frac{a}{W})(1 - \frac{a}{W})^{3/2}} \quad (2)$$

Modules I fracture toughness (K_{Ic}) was determined from the maximum applied load recorded during test and the initial notch length.

Three-Point Bend Coupled with Micro-CT

Incremental three-point bending tests were performed on one 5 vol.% and one 25 vol.% epoxy-alumina specimens using a loading device (CT5000, Deben, Suffolk, UK) coupled with micro-CT (Phoenix v|tome|x L300, GE, Boston, MA) (Fig. 1c). The specimen geometry, loading span and the displacement rate were the same as previously described in “Three-Point Bend Using Conventional Mechanical Tester” section. 0.1 mm/min is the lowest displacement rate in the loading device coupled with micro-CT.

The tests were performed under displacement control and were paused discretely, when the loading frame was held still for 20–30 min to allow the specimen to fully relax. After stress-relaxation, micro-CT scans were then performed using 140 kV voltage, $35 \mu\text{A}$ current and isometric voxel size of $8 \mu\text{m}$. Each scan took about 30 min. For each specimen, the tests were paused for 5–6 times for micro-CT scans, until they fractured completely or until the load dropped to zero.

The load and displacement were recorded by the tester. The corresponding incremental crack growths were measured from the micro-CT images, using the longest crack length in all image slides. The crack growth resistance (R-curves) were determined using Eqs. 1 and 2 using the loads recorded at the moment when the tests were just paused without stress-relaxation.

The micro-CT image stacks were segmented using image processing software Avizo (FEI Visualization Sciences Group, Burlington, MA). The specimen, notch and crack were labeled, respectively. 3D images were generated using volume rendering algorithm to visualize the cracks in 3D. Two-dimensional (2D) micro-CT image slices were examined to determine the crack paths and toughening mechanisms.

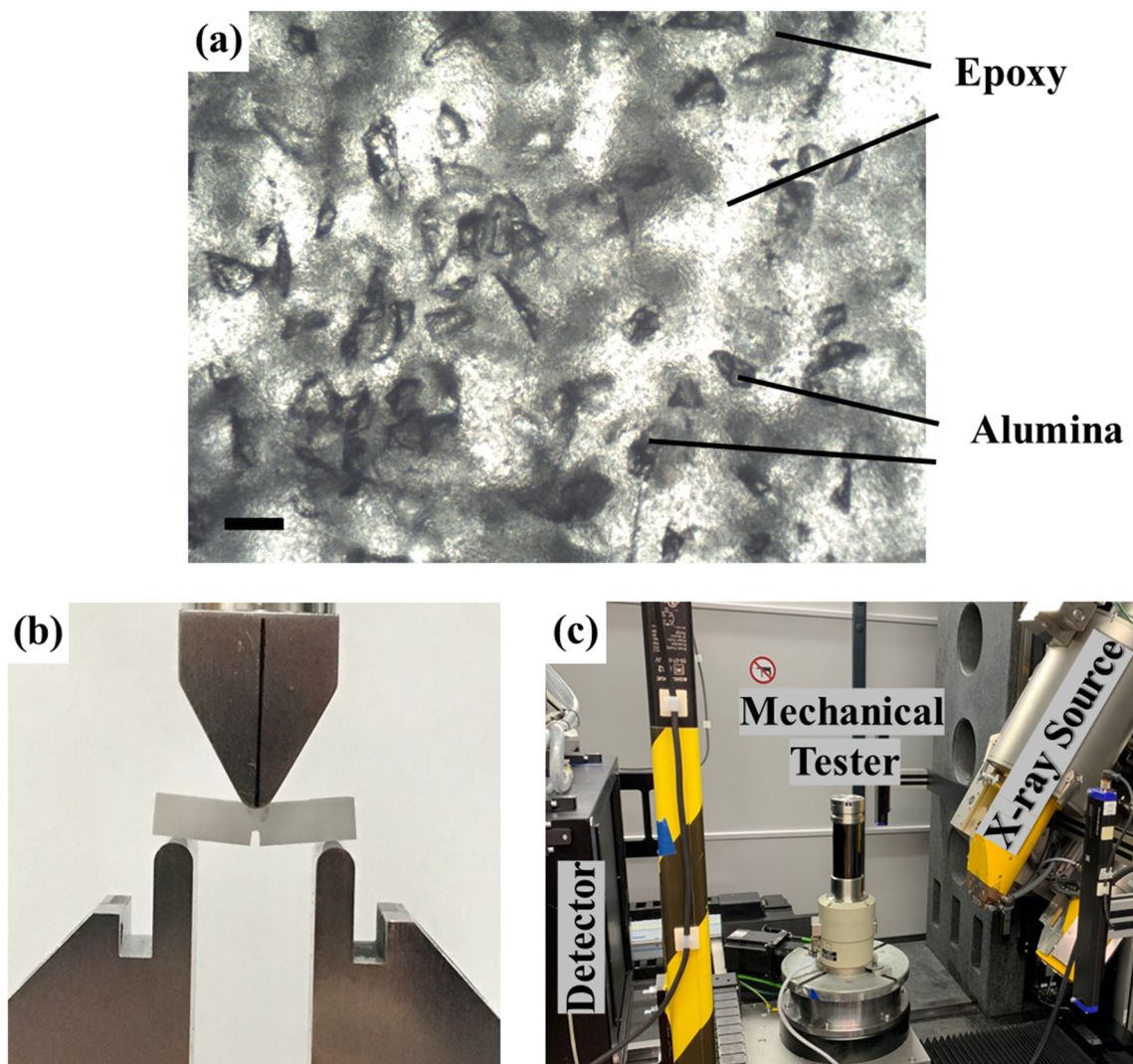


Fig 1. (a) Optical image of a thin slice of specimen (Scale bar 100 μm). (b) Experimental setup for 3-point bending test on epoxy-alumina SENB specimens using a conventional mechanical tester and (c) an in situ mechanical tester coupled with micro-CT.

RESULTS AND DISCUSSION

Load-Displacement Curves

The load-displacement curves recorded by conventional mechanical tester during three-point bending tests of epoxy-alumina are presented in Fig. 2a. One representative specimen was chosen for each volume fraction that it exhibited the fracture toughness closest to the average value for the group. As the filler fraction of the composites increased, the stiffness (slope of load-displacement curves) also increased. On the other hand, the maximum load reduced with increasing filler fraction. The displacement corresponding to the maximum load also reduced with increasing filler fraction. Several researchers have reported that the modulus for epoxy-alumina composite increased with increasing filler fraction.^{13,16,17} Shukla et al.¹³ have also reported that the strength and failure strain in the uniaxial tensile tests for epoxy-alumina

composite decreased with increasing filler fraction. These are in good agreement with the load-displacement curves obtained in this study.

The load-displacement curves also showed that pure epoxy specimens fractured immediately after the maximum load was reached; 5 vol.% epoxy-alumina specimens deformed a little after the maximum load was reached and then fractured; 10–25 vol.% epoxy-alumina specimens kept deforming after the maximum load was reached and did not fully fracture even after the load dropped to almost 0.

Fracture Toughness

The fracture toughness of pure epoxy was measured to be $3.46 \text{ MPa}\sqrt{\text{m}}$, whereas other studies reported the fracture toughness of epoxy to be between 0.58 and $1.51 \text{ MPa}\sqrt{\text{m}}$.^{13,16,18} The higher toughness value reported in this study may be attributed to the different type of epoxy used than

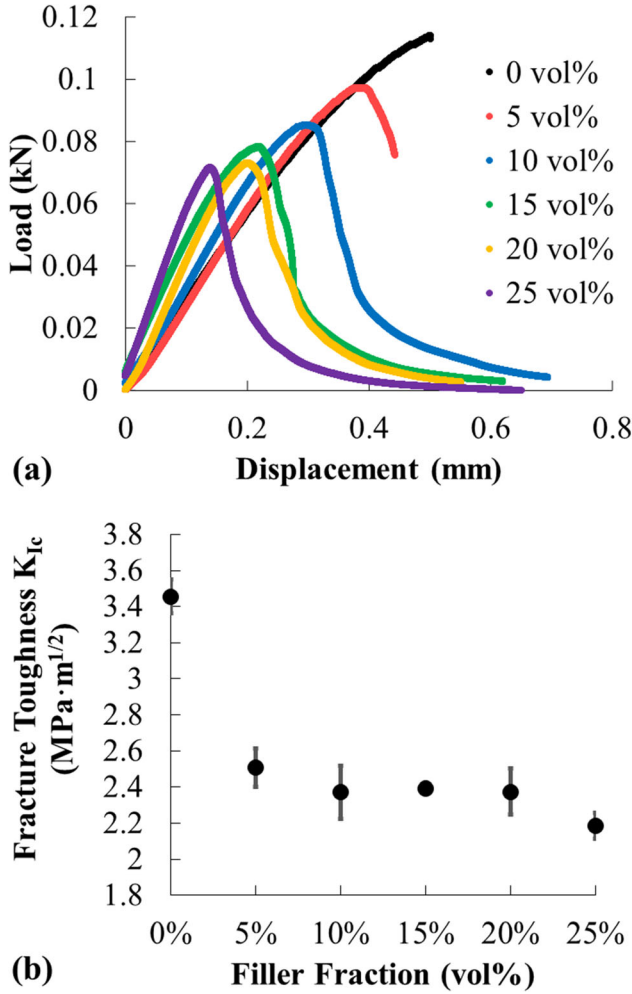


Fig 2. (a) Load-displacement curves and (b) fracture toughness values obtained from 3-point bending test for epoxy-alumina SENB specimens with various filler fractions.

other studies. It can also be attributed to the blunt notch in the SENB specimen in this study. Besides the specimens prepared in “Sample Preparation” section, some other specimens SENB specimens were prepared with a sharp pre-crack introduced by a razor blade. However, the metallic debris trapped in the notch caused severe beam-hardening artifacts in the micro-CT images and hindered other image-based measurements and characterizations. A direction for future work would be creating sharp pre-crack in SENB specimens without introducing metallic debris.

Fracture toughness of epoxy-alumina was measured to be between 2.10 and 2.51 MPa√m, and it decreased with increasing filler fraction, as shown in Fig. 2b. Marur et al.¹⁹ reported that the fracture toughness of epoxy-alumina first decreased with increasing filler fraction from 5 vol.% to 25 vol.% and then increased when the filler fraction increased to 30–40 vol.%. There were also other studies showed that the fracture toughness of the epoxy-alumina increased with increasing filler

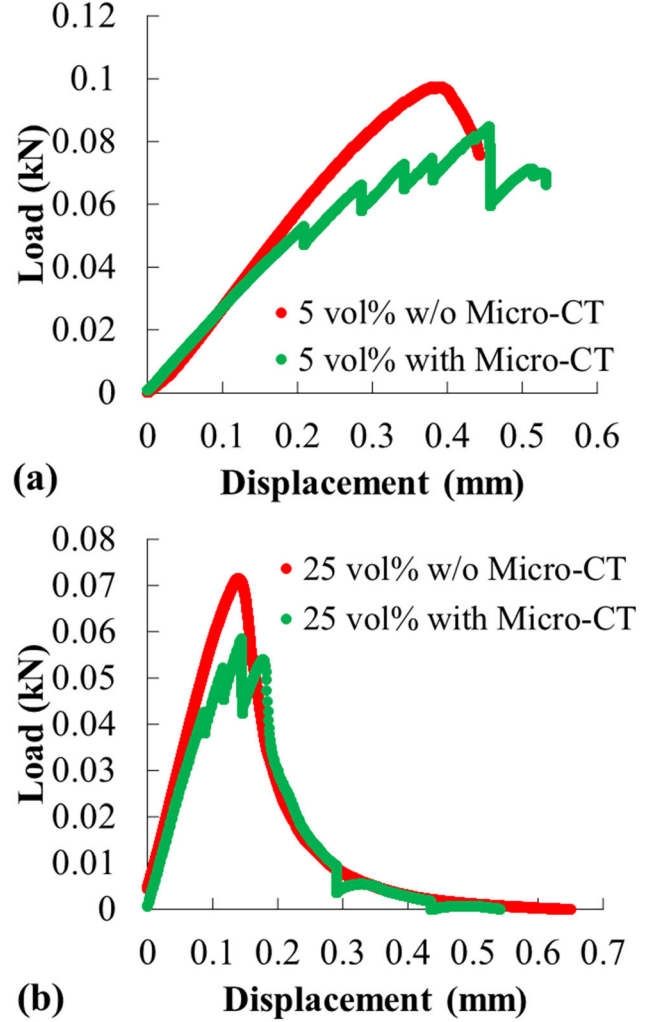


Fig 3. Comparison of load-displacement curves obtained from 3-point bending test in a conventional mechanical tester and in an in situ mechanical tester coupled with micro-CT: (a) 5 vol.% and (b) 25 vol.% epoxy-alumina SENB specimens.

fraction from 1 vol.% to 50 vol.%.^{13,16,18} The different trends reported in these literatures and in this study can be attributed to the different types of epoxy resin the much smaller or to the fact that the 80 μm alumina fillers in this study are much bigger than the sub-micron or nano-scale fillers in the above-mentioned literatures.

Crack Growth Resistance (R-curves)

The load-displacement curves recorded during the incremental three-point bending tests coupled with micro-CT are presented in Fig. 3. They are compared with the load-displacement curves recorded in the tests using conventional tester (Fig. 3). The initial loading portions of the curves with and without coupling with micro-CT were overlapping. When the tests were paused, the loading frame was held still and the applied load on the specimen reduced during stress relaxation. Hence the load recorded in the tests coupled with micro-CT was

lower than that in the conventional tests (Fig. 3). When the tests went past the maximum load, the load-displacement curves with and without coupling with micro-CT overlapped again, especially for the 25 vol.% epoxy-alumina specimen.

Although the same displacement rate was used in the 3-point bending tests without and with micro-CT scans, the time length deferred in the two types of testing, due to the holding and micro-CT scans in the tests coupled with micro-CT. This could contribute to the differences in the load-displacement curves (Fig. 3). The effects of loading rate need to be explored in future works.

Micro-CT images taken during the incremental three-point bending tests coupled with micro-CT are presented in Fig. 4. The 5 vol.% specimen was scanned five times when the displacement was 0.21, 0.29, 0.34, 0.38, and 0.46 mm, respectively. It then fractured when the displacement reached 0.53 mm (Fig. 3a). The 25 vol.% specimen was scanned six times when the displacement was 0.09, 0.12, 0.15, 0.29, 0.44 and 0.58 mm, respectively (Fig. 3b). At 0.58 mm displacement, the load dropped to about zero, but the specimen did not fully fracture. These are consistent with observations in the conventional

3-point bending test without micro-CT scans (“Load-Displacement Curves” section).

Micro-CT image slices at the same locations inside the specimens at each incremental step are compared (Fig. 4). During the test, multiple cracks developed from the notch and propagated into the specimens. The crack length, Δa , from the notch to the tip of the longest crack inside the specimens (arrows in Fig. 4) were measured from the image slices to be 0.14 mm, 0.31 mm, 0.58 mm, 0.76 mm and 1.04 mm for 5 vol.% epoxy-alumina and 0 mm, 0.29 mm, 0.88 mm, 1.94 mm and 2.20 mm for 25 vol.% epoxy-alumina, respectively.

The crack growth resistance curves (R-curves) for the 5 vol.% and 25 vol.% epoxy-alumina composites are given in Fig 5. The results show that the two composites had similar crack-initiation toughness around $1.33 \text{ MPa}\sqrt{\text{m}}$. The crack resistance capabilities for the two composites were also similar, when the cracks were shorter than 0.88 mm. When the crack length was greater than 0.88 mm, the 25 vol.% epoxy-alumina exhibited no crack resistance, with the stress intensity factor first remained constant and then decreased with crack extension. In contrast, stress intensity factor kept increasing in 5 vol.% epoxy-alumina and the slope of the R-curves

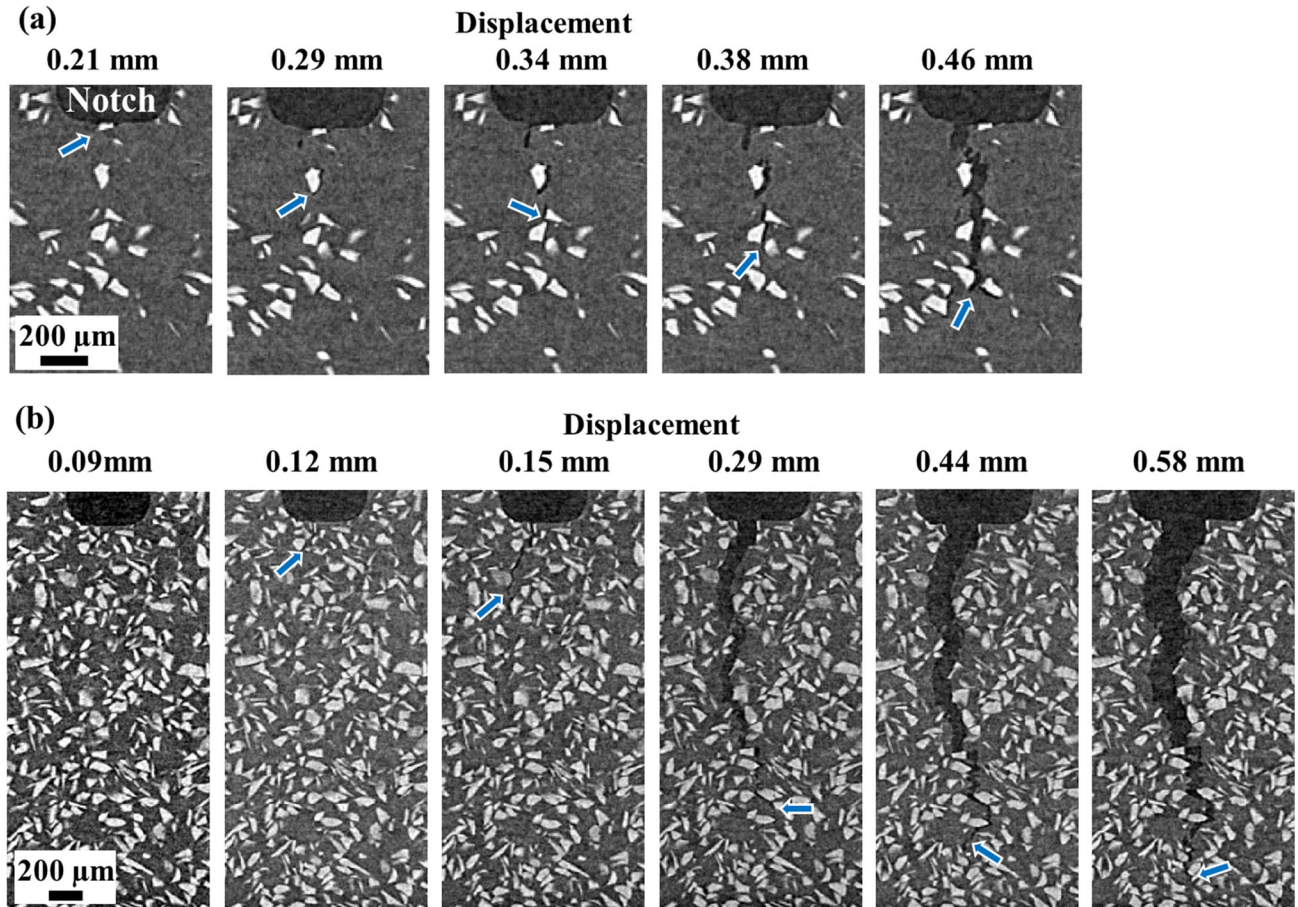


Fig 4. Micro-CT image slices showing the crack growth in (a) 5 vol.% and (b) 25 vol.% epoxy-alumina SENB specimens at different stages during 3-point bending test. Arrows are pointing at the crack tips.

even slightly increased with increasing crack length.

Crack Paths and Toughening Mechanisms

3D volume rendered images revealed the 3-dimensional development of cracks inside the materials (Fig. 6). To better visualize the cracks, only a section of the specimens near the longest crack was presented. The images (Fig. 6) show that multiple one-dimensional (1D) needle-shape cracks initiated from the notch (0.21 mm displacement); while extending into the materials, they also extended in the thickness direction of the specimen and became 2D plate shape (0.29 mm displacement); multiple cracks extended at the same time while new cracks initiated from the notch (0.34 mm displacement); these cracks had different lengths and the longest crack can be considered as the main crack (0.38 mm displacement); crack coalescences can be observed at the final stages of damage (0.46 mm displacement).

The 2D micro-CT image slices show the typical crack paths inside the materials (Fig. 7a). Cracks propagated through the epoxy matrix, through the alumina particles, and also along the particle-matrix interfaces. Cracks going through the alumina particles and causing particle fracture were observed less frequently than other cases.

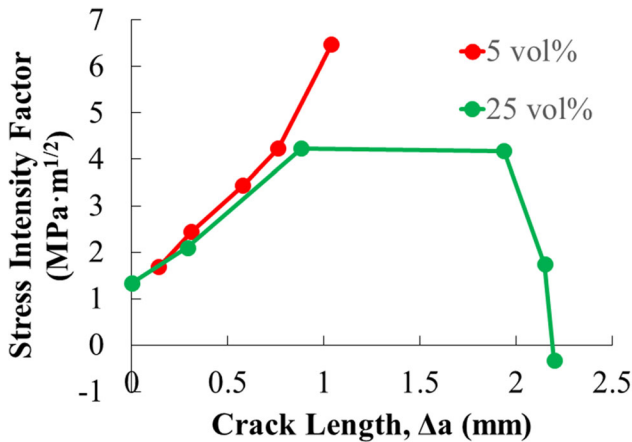


Fig 5. Crack-resistance curves for epoxy-alumina composites.

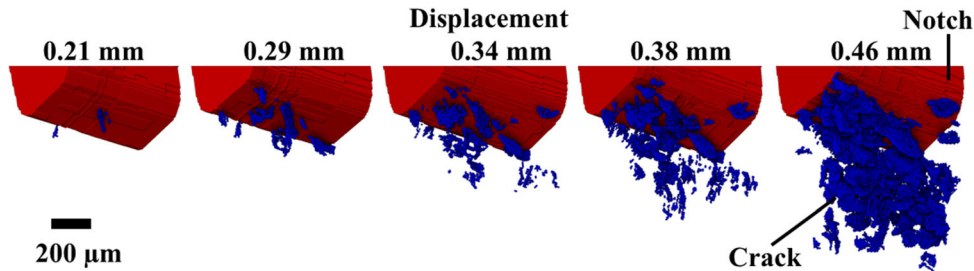


Fig 6. 3D volume rendered micro-CT images for a 5 vol.% epoxy-alumina SENB specimen at different stages during 3-point bending test. Red—notch; blue—cracks. The specimen was rendered fully transparent for better presentation of the cracks.

The 2D micro-CT image slices also show several toughening mechanisms for epoxy-alumina composites. Crack deflection was a commonly observed toughening mechanism. It can be seen in Figs. 4b and 7b. Crack bridging by uncracked ligament was also common (Figs. 4a and 7c). Crack bridging by the filler particles can be seen in Fig. 7d, but it was not commonly observed. Additionally, the 3D volume rendered images (Fig. 6) demonstrated toughening by micro-cracks.

Implications

The current results suggest that the matrix-particle interface is the weakest link in the epoxy-alumina composites. The damage initiated from debonding of matrix-particle interfaces, which can be contributed to the stress concentration at the interfaces or to the low interface strength. The fracture toughness decreased with increasing filler fraction, because the weakest link, matrix-particle interfaces, increased in the materials, and because the crack bridging by uncracked filament was reduced. To design robust epoxy-alumina composites, increasing matrix-particle interface strength is recommended as a direction for future work.

The conventional methods to visualize crack morphology and exam the fracture surfaces include optical microscope and scanning electron microscopy (SEM).^{13,16,18,20,21} transmission electron microscopy^{22–26} and atomic force microscopy (AFM).²² They can only examine the specimen surfaces or fracture surfaces. Sometimes, specimens need to be cut and sectioned to visualize the internal damage and cracks. An advantage of x-ray based microscope techniques is that they can be used to image the internal structures, including cracks, without cutting and sectioning the specimens. The limitations of these methods include the possible damage to the specimens due to radiation. Among these techniques, micro-CT is more accessible than SR-CT, but it often requires a longer scanning time and results in images with greater voxel size than SR-CT. The results of current study show that the image quality of micro-CT is good enough for the study of 3D crack growth in polymer-ceramic composites.

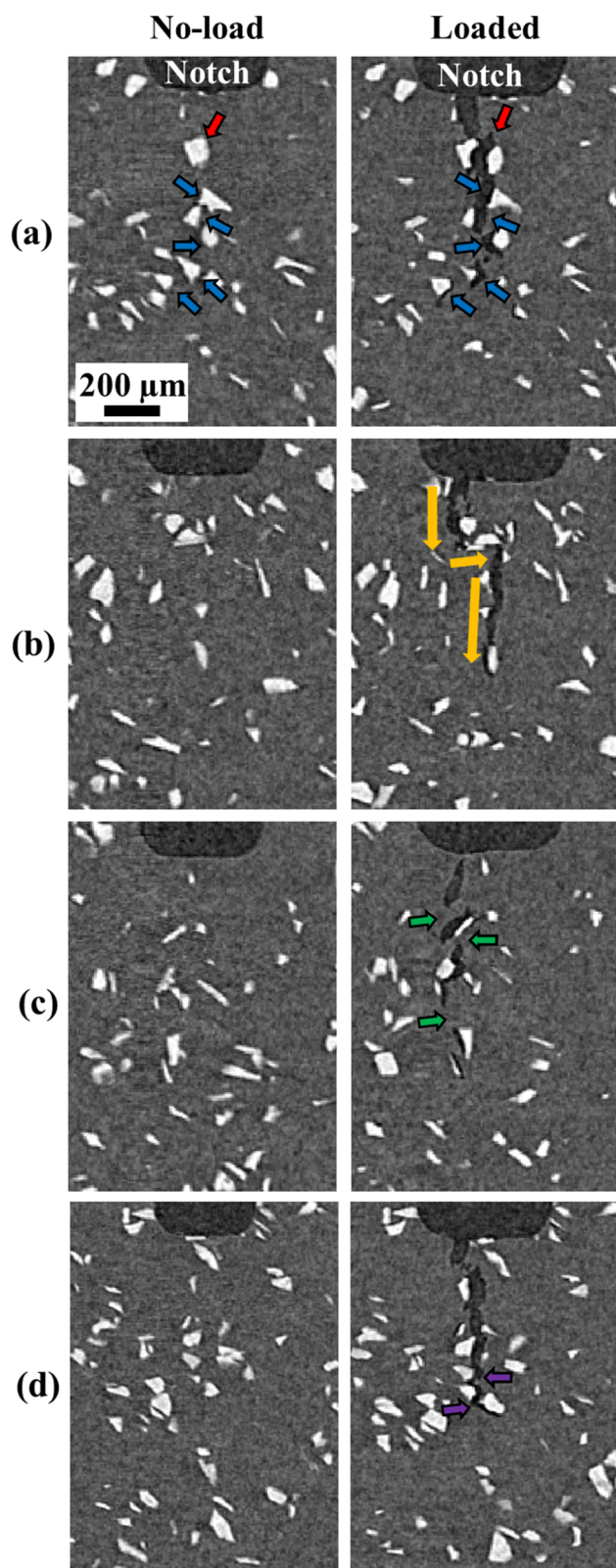


Fig 7. Comparison of micro-CT images of 5 vol.% epoxy-alumina taken at no-loaded and loaded conditions showing (a) the crack growth paths through the matrix, across the particles (red arrow) and at the matrix-particle interfaces (blue arrows), (b) crack deflection toughening, (c) crack bridging by uncracked ligament and (d) crack bridging by the fillers (Color figure online).

In ex situ studies, measurements were often carried out after the specimens were fully fractured or when applied load was removed. The in situ method used in this study allowed imaging while the mechanical loads were applied on the specimens, when the cracks were open and easy to visualize in the images. The in situ method used in this study also enabled the tracking of crack growth process at the same micro-scale locations at different stages of loading.

CONCLUSION

This paper presented the results of an investigation on the internal cracks in epoxy-alumina composite materials using in situ mechanical testing coupled with micro-CT. Fracture toughness was measured by three-point bending test to be between 2.10 and 2.51 $\text{MPa}\sqrt{\text{m}}$ for epoxy-alumina with alumina fillers between 5 vol.% and 25 vol.%, and it decreased with increasing filler fraction. The crack resistance capabilities for 5 vol.% and 25 vol.% composites were similar, when the cracks were shorter than 0.88 mm. When the crack length was greater than 0.88 mm, the 25 vol.% epoxy-alumina exhibited no crack resistance. In contrast, stress intensity factor kept increasing in 5 vol.% epoxy-alumina.

The matrix-particle interfaces were the weakest link in the materials, where the cracks often initiated from. The crack bridging by uncracked ligament and crack deflection were the commonly observed toughening mechanisms. Other toughening mechanisms include crack bridging by filler particles and micro-cracks toughening. To design robust epoxy-alumina composites, increasing matrix-particle interface strength is recommended as a direction for future work.

ACKNOWLEDGEMENTS

This research is supported by the National Science Foundation (#1826221). The authors are grateful to the program manager, Dr. Siddiq Qidwai, for his encouragement and support. Appreciation is extended to Dr. Timothy Stecko of Penn State Center for Quantitative Imaging for technical assistance with micro-CT scanning.

CONFLICT OF INTEREST

The authors declare that they have no conflict of interest.

REFERENCES

1. D. Mohamad Yunos, O. Bretcanu, and A.R. Boccaccini, *J. Mater. Sci.* 43, 4433. (2008).
2. H. Qiu, J. Yang, P. Kodali, J. Koh, and G.A. Ameer, *Biomaterials* 27, 5845. (2006).
3. V. Mouriño, J.P. Cattalini, J.A. Roether, P. Dubey, I. Roy, and A.R. Boccaccini, *Expert Opin. Drug Deliv.* 10, 1353. (2013).
4. J. Du, X. Niu, N. Rahbar, and W. Soboyejo, *Acta Biomater.* 9, 5273. (2013).

5. J. Du, X. Niu, and W. Soboyejo, *J. Mech. Behav. Biomed. Mater.* 46, 41. (2015).
6. J.J. Kruzic, R.K. Nalla, J.H. Kinney, and R.O. Ritchie, *Biomaterials* 24, 5209. (2003).
7. R.K. Nalla, J.J. Kruzic, J.H. Kinney, and R.O. Ritchie, *Biomaterials* 26, 217. (2005).
8. P.J. Schilling, B.R. Karedla, A.K. Tatiparthi, M.A. Verges, and P.D. Herrington, *Compos. Sci. Technol.* 65, 2071. (2005).
9. A.J. Moffat, P. Wright, J.Y. Buffière, I. Sinclair, and S.M. Spearing, *Scr. Mater.* 59, 1043. (2008).
10. B. Croom, W.M. Wang, J. Li, and X. Li, *Exp. Mech.* 56, 999. (2016).
11. Y. Zhou, C. Gong, G.S. Lewis, A.D. Armstrong, and J. Du, *Extrem. Mech. Lett.* 35, 100614. (2020).
12. Y. Zhou, C. Gong, M. Hossaini-Zadeh, and J. Du, *J. Mech. Behav. Biomed. Mater.* 110, 103858. (2020).
13. D.K. Shukla, and V. Parameswaran, *J. Mater. Sci.* 42, 5964. (2007).
14. ASTM E399, *Standard Test Method for Linear-Elastic Plane-Strain Fracture Toughness K_{1C} of Metallic Material* (2013).
15. J.E. Srawley, *Int. J. Fract.* 12, 475. (1976).
16. L.M. McGrath, R.S. Parnas, S.H. King, J.L. Schroeder, D.A. Fischer, and J.L. Lenhart, *Polymer (Guildf)*. 49, 999. (2008).
17. S. Zhao, L. Schadler, R. Duncan, H. Hillborg, and T. Auletta, *Compos. Sci. Technol.* 68, 2965. (2008).
18. D. Shukla, S. Kasisomayajula, and V. Parameswaran, *Compos. Sci. Technol.* 68, 3055. (2008).
19. P.R. Marur, R.C. Batra, G. Garcia, and A.C. Loos, *J. Mater. Sci.* 39, 1437. (2004).
20. A. Omrani, L.C. Simon, and A.A. Rostami, *Mater. Chem. Phys.* 114, 145. (2009).
21. O. Jin, Y. Li, and W.O. Soboyejo, *Appl. Compos. Mater.* 5, 25. (1998).
22. B. Wetzels, P. Rosso, F. Hauptert, and K. Friedrich, *Eng. Fract. Mech.* 73, 2375. (2006).
23. J. Douce, J.P. Boilot, J. Biteau, L. Scodellaro, and A. Jimenez, *Thin Solid Films* 466, 114. (2004).
24. M.C. Kuo, C.M. Tsai, J.C. Huang, and M. Chen, *Mater. Chem. Phys.* 90, 185. (2005).
25. L. Jiang, J. Zhang, and M.P. Wolcott, *Polymer (Guildf)*. 48, 7632. (2007).
26. Y. Chen, S. Zhou, H. Yang, and L. Wu, *J. Appl. Polym. Sci.* 95, 1032. (2005).

Publisher's Note Springer Nature remains neutral with regard to jurisdictional claims in published maps and institutional affiliations.